HHS Public Access

Author manuscript

Aging Brain. Author manuscript; available in PMC 2022 April 22.

Published in final edited form as:

Aging Brain. 2022 ; 2: . doi:10.1016/j.nbas.2022.100039.

Cerebral topography of vesicular cholinergic transporter changes in neurologically intact adults: A [18F]FEOBV PET study

Prabesh Kanel[a,b,*], **Sygrid van der Zee**[c], **Carlos A. Sanchez-Catasus**[d,e], **Robert A. Koeppe**[a], **Peter J.H. Scott**[a], **Teus van Laar**[c], **Roger L. Albin**[b,f,g], **Nicolaas I. Bohnen**[a,b,f,g]

[a]Department of Radiology, University of Michigan, Ann Arbor, MI, USA

[b]University of Michigan Morris K. Udall Center of Excellence for Parkinson's Disease Research, Ann Arbor, MI, USA

[c]Department of Neurology, University Medical Center Groningen, Groningen, the Netherlands

[d]Department of Neurology, Clinica Universidad de Navarra, 31008 Pamplona, Spain

[e]Department of Nuclear Medicine and Molecular Imaging, University Medical Center Groningen, the Netherlands

[f]Department of Neurology, University of Michigan, Ann Arbor, MI, USA

[g]Neurology Service and GRECC, VAAAHS, Ann Arbor, MI, USA

Abstract

Acetylcholine plays a major role in brain cognitive and motor functions with regional cholinergic terminal loss common in several neurodegenerative disorders. We describe age-related declines of regional cholinergic neuron terminal density *in vivo* using the positron emission tomography (PET) ligand [^{18}F](–)5-Fluoroethoxybenzovesamicol ([^{18}F] FEOBV), a vesamicol analogue selectively binding to the vesicular acetylcholine transporter (VAChT). A total of 42 subjects without clinical evidence of neurologic disease (mean 50.55 [range 20–80] years, 24 Male/18 Female) underwent [^{18}F]FEOBV brain PET imaging. We used SPM based voxel-wise statistical

*Corresponding author at: Functional Neuroimaging, Cognitive and Mobility Laboratory, Departments of Radiology and Neurology, University of Michigan, 24 Frank Lloyd Wright Drive, Box 362, Ann Arbor, MI 48105-9755, USA. prabeshk@umich.edu (P. Kanel).

Declaration of Competing Interest

Dr. Koeppe has received grant support from the National Institute of Health, the Farmer Family Foundation Parkinson's Research Initiative and National Institute of Aging.

Dr. Scott has received grant from U.S. Department of Energy, the National Institute of Biomedical Imaging and Bioengineering, the Farmer Family Foundation Parkinson's Research Initiative and the Alzheimer's Association, AbbVie and Bristol-Myers Squibb.

Dr. Frey has research support from the National Institutes of Health, National Institute of Neurological Disorders and Stroke, National Cancer Institute, GE Healthcare and AVID Radiopharmaceuticals (Eli Lilly subsidiary). Dr. Frey also serves as a consultant to AVID Radiopharmaceuticals, MIMVista, Inc, Bayer-Schering and GE healthcare. He also holds equity (common stock) in GE, Bristol-Myers, Merck and Novo-Nordisk.

Dr. van Laar has received research support from the Weston Brain Institute, speaker fees from Brittania and is on the advisory boards of Brittania and AbbVie, Medtronic and is on the advisory boards of LTI and Neuroderm.

Dr. Albin has research support from the National Institute of Neurologic Disease and Stroke, the Parkinson's Foundation, the National Institute on Aging, and the Farmer Family Foundation Parkinson's Research Initiative.

Dr. Bohnen has research support from the National Institute of Health, Department of Veteran Affairs, the Parkinson's Foundation, and the Farmer Family Foundation Parkinson's Research Initiative.

The remaining authors declare that they have no known competing financial interests or personal relationships that could have appeared to influence the work reported in this paper.

analysis to perform whole brain voxel-based parametric analysis (family-wise error corrected, FWE) and to also extract the most significant clusters of regions correlating with aging with gender as nuisance variable. Age-related VAChT binding reductions were found in primary sensorimotor cortex, visual cortex, caudate nucleus, anterior to mid-cingulum, bilateral insula, *para*-hippocampus, hippocampus, anterior temporal lobes/amygdala, dorsomedial thalamus, metathalamus, and cerebellum (gender and FWE-corrected, $P < 0.05$). These findings show a specific topographic pattern of regional vulnerability of cholinergic nerve terminals across multiple cholinergic systems accompanying aging.

Keywords

Acetylcholine transporter; Aging; Normal persons; VAChT PET

Introduction

Normal aging is associated with cholinergic system losses in the brain (see [1–3] for review). Most data relevant to age-related declines of cholinergic systems derives from older post-mortem studies of the basal forebrain cholinergic corticopetal complex (BFCC) evaluating markers of cholinergic terminal and perikaryal integrity [3]. Other important brain cholinergic systems were largely ignored in these studies.

Important cholinergic projection systems include the BFCC, notably the nucleus basalis of Meynert (nbM), which provides the principal cholinergic input of the entire cortical mantle and amygdala [4]. The medial septal and vertical limb of the diagonal band nuclei of the BFCC innervate the hippocampal formation. The pedunculopontine nucleus/lateral dorsal tegmental complex (PPN/LDTC) provides cholinergic inputs to the basal ganglia, thalamus, cerebellum, several brainstem nuclei, and the spinal cord [5]. The medial vestibular nucleus (MVN) is a major source of cholinergic input to the cerebellum [6]. The striatum exhibits the highest density of cholinergic terminal markers in the brain. Cholinergic nerve terminals in the striatum may derive from striatal cholinergic interneurons (SChIs) or from extrinsic projections from the PPN/LDTC, with available evidence indicating that the great majority of striatal cholinergic terminals emanate from SChIs [7,8]. There is a paucity of information about the relationship between normal aging and changes in brain cholinergic systems other than the BFCC. Our recent positron emission tomography (PET) study using the vesicular acetylcholine transporter (VAChT) ligand [^{18}F](–)5-fluoroethoxybenzove samicol ([^{18}F]FEOBV) found significant age-associated decreases in [^{18}F]FEOBV binding in striatum (approximately 4% binding loss per decade) and approximately 2.5% per decade FEOBV binding losses in primary sensorimotor cortex, anterior cingulum, and thalamus of neurologically intact adults [9]. VAChT expression is unique to cholinergic terminals and [^{18}F]FEOBV PET is thought to be a specific and robust measure of regional cholinergic terminal density [10]. Assessment of aging effects in this study was based on limited volume-of-interest analysis using a *priori* selection of relatively high binding regions. This approach lacks sensitivity to assess cholinergic aging effects in regions with lower tracer binding and also in characterizing changes within larger preselected volumes-of-interest, such as the striatum. A more systematic analysis requires a spatially unbiased approach.

The goal of this paper is to perform a whole brain voxel-based analysis to investigate the topography of age-related cholinergic terminal changes using [^{18}F]FEOBV PET in normal adults and across a wide age range and complemented by a cluster peak analysis. Identification of the topographic vulnerability of cholinergic systems during aging is relevant to understand the contributions of normal aging to age-related neurodegenerative disorders exhibiting cholinergic systems degenerations, such as Parkinson's or Alzheimer's disease. Identifying the topography of normal age-related changes in cholinergic systems may also be relevant to understand potential sensitivity to the use of commonly prescribed anticholinergic drugs in older adults.

Subjects and methods

Subjects

This cross-sectional study involved 42 neurologically intact normal control subjects (24 males, 18 females), mean age 50.55 ± 19.35, age range 20–80 years. Data from 29 subjects was used in a previous study describing the normal biodistribution of VAChT binding with limited (volume-of-interest method only) aging effects analyses [9]. Ten subjects (5/5 M/F) out of 42 were part of the Dutch Parkinson Cohort (DUPARC) study [11]. No subjects had histories of the neurologic or psychiatric disease, none took medications that might affect cholinergic neurotransmission (either cholinergic or anticholinergic drugs) and all had a normal neurological examination at the time of this study. The study was approved by and study procedures were followed in accordance with the ethical standards of the Institutional Review Board of the University of Michigan and medical ethical committee of the University of Groningen. Written informed consent was obtained from all subjects.

Imaging techniques—All subjects underwent brain MRI and VAChT [^{18}F]FEOBV PET imaging. MRI was performed on a 3 Tesla Philips Achieva system (Philips, Best, The Netherlands) at the University of Michigan and a 3 Tesla Philips Intera system (Philips, The Netherlands) at the University Medical Center Groningen (UMCG). PET imaging was performed in 3D imaging mode with an ECAT Exact HR + tomograph (Siemens Molecular Imaging, Inc., Knoxville, TN) as previously reported [12] or Biograph 6 TruPoint PET/CT scanner (Siemens Molecular Imaging, Inc., Knoxville, TN) as previously described [13] at the University of Michigan and Biograph 40-mCT or 64-mCT TruPoint PET/CT scanner (Siemens Molecular Imaging, Inc., Knoxville, TN) at the UMCG as previously described [11]. [^{18}F] FEOBV were prepared as described previously [14]. Inter-camera data harmonization was performed as described [15]. We constructed TruePoint images with 3 mm filters to match the resolution and to account for differences between the scanners. To reduce the scanner variability, the acquisition parameters used at the University of Michigan were followed at the UMCG. We reconstructed all [^{18}F] FEOBV PET images obtained at the UMCG using software, methodology and reconstruction parameters identical to those used at the University of Michigan.

Image analysis

Spatial preprocessing—We constructed parametric images to reflect Distribution Volume Ratios (DVR) of [^{18}F] FEOBV in the brain by using the supratentorial white

matter as a reference region as previously reported [16–18]. All structural MRI images were segmented into native and 'Dartel-imported' gray matter, white matter and cerebrospinal fluid using the Statistical Parametric mapping 12 (SPM12) software package (https://www.fil.ion.ucl.ac.uk/spm/). Using this segmentation, a Muller-Gartner partial-volume correction method was used to remove the partial volume effect (PVE) on our PET images [19]. Each subject's structural MRI along with registered PVE corrected PET image is then normalized to the study specific template in Montreal Neurological Institute (MNI) space using high-dimensional DARTEL registration. To remove random noise, normalized PVE corrected PET images were spatially smoothed to 8 mm full width at half maximum (FWHM). We performed the images preprocessing steps from both the centers at the University of Michigan. Before including the Groningen subjects in our analysis and to account for any biases present in the images due to scanning at two sites, we applied an inter-scanner normalization method as listed above [15] between age and gender-matched subjects between the center and found no significant difference between any of the images. The mask of the basal forebrain in MNI space was drawn from a multilevel atlas framework based on the Julich Brain atlas (https://www.fz-juelich.de/inm/inm-1/EN/Forschung/JulichBrain/JulichBrain_Webtools/JulichBrain_Webtools_node.html) using the previously described method [20–22].

Statistical analysis

To evaluate the effect of neurologically intact adults on [^{18}F] FEOBV DVR in the brain, a voxel-based correlation analysis of the parametric images in MNI space was performed using SPM12, with age as the variance of interest and gender as the nuisance covariate. Both positive and negative correlations were evaluated. A cluster-based analysis was also performed and statistical parametric mapping results were thresholded at voxel level $p < 0.001$ and corrected for whole-brain comparisons using cluster-level family-wise error rate ($p < 0.05$). Clusters that survived the cluster-level family-wise error rate were interpreted as significant.

Results

Age-related reductions of VAChT binding were found in primary sensorimotor cortex, visual cortex, caudate nucleus, anterior to mid cingulum, bilateral insulae, *para*-hippocampus, hippocampus, anterior temporal lobes/amygdala, metathalamus (lateral and medial geniculate nuclei), dorsomedial thalamus, and cerebellum (gender and FWE-corrected, $P < 0.05$; Fig. 1).

Scatter plots of distribution volume ratio of parahippocampal gyrus and caudate nucleus show age-associated reductions of VAChT binding (Fig. 2). Similarly, a voxel-based morphometric analysis of the basal forebrain detects age-related reduction of volume in basal forebrain in neurologically intact adults, gender and FWE-corrected, $P < 0.05$ (Fig. 3).

Table 1 lists the major clusters with cluster size 50 voxels or more, FWE-corrected p-values, the coordinates (X, Y, Z) of the local maxima within that cluster in MNI space, peak voxel z and t-score at the local maxima, and brain regions associated with the clusters.

Discussion

Post-mortem studies show that neurologically intact control persons exhibit age-related declines of BFCC perikaryal density, and within the cortex, in biochemical and histochemical markers of cholinergic terminal density. Other cholinergic systems are less studied. Molecular imaging methods allow *in vivo* evaluation of cholinergic systems integrity but there is only scarce *in vivo* molecular imaging data on the relationships between normal aging and cholinergic systems integrity. A prior VAChT ligand ^{123}I-iodobenzovesamicol (IBVM) single photon emission computed tomography (SPECT) imaging study in neurologically intact controls found cortical IBVM binding declined 3.7% per decade between the ages of 21 and 91 [23]. The limited resolution of SPECT precluded more detailed analysis and results in subcortical structures were not reported. A $\alpha_4\beta_2$ ^{123}I-5-IA-85380 SPECT study of nicotinic cholinergic receptors found an inverse correlation between age and receptor binding availability in neurologically intact adults aged 18–85 years [24]. Declines ranged from 32% (thalamus) to 18% (occipital cortex) over the adult lifespan, or up to 5% per decade, but these results may partly reflect post-synaptic changes. Our more recent VAChT [^{18}F]FEOBV PET study, with a subset of the normal participants (n = 29) used for this analysis, found significant age-associated decreases in [^{18}F]FEBOV binding of the striatum (approximately 4% binding loss per decade) with approximately 2.5% per decade binding losses in the primary sensorimotor cortex, the anterior cingulum, and the thalamus. Other regions did not show significant age-related reductions [9].

Our current analysis, performed with a larger study sample and using a whole-brain voxel-based analysis method, as opposed to the volumes-of-interest analyses of prior studies, confirms our prior results and depicts a more granular topography of age-related cholinergic terminal declines. Novel findings include preferential vulnerability of the caudate nucleus cholinergic terminals relative to those of the putamen, and similar relative vulnerability of the metathalamus cholinergic terminals compared to those of the thalamus. Other novel findings include age-related declines of [^{18}F]FEOBV binding in hippocampal and parahippocampal regions, the calcarine cortex, and parts of the cerebellar cortex. The striatal and cerebellar results show the potential strengths of this voxel-by-voxel analysis. The striatal cluster of significant voxels suggests preferential involvement of caudate SChIs. The prior volume-of-interest analysis did not detect any changes in the cerebellum, even in regions of high [^{18}F] FEOBV binding such as nodulus and flocculus.

A FEOBV PET study of aging rodents [25] found aging associated with hippocampal and parietotemporal cortical cholinergic losses. Our study in neurologically intact adults found evidence of more widespread age-related losses extending beyond these regions. This may either reflect a critical difference between rodents and the human brain versus more detailed neuroimaging analysis techniques applied to the anatomically larger human brain.

Our present results indicate age-related changes in all major brain cholinergic systems, including declines of BFCC terminals, PPN-LDTC cholinergic terminals, MVN cholinergic terminals, and likely SChI terminals. Our findings suggest that the BFCC afferents to limbic and paralimbic cortices appear more vulnerable than BFCC afferents to most of the neocortex with the exception of primary sensorimotor and calcarine cortices. These

results suggest preferential age-related effects on medial septal/vertical limb of the diagonal band nucleus and nBM subpopulations. Recent studies indicate that the BFCC is not a diffuse projections system but rather composed clusters of cholinergic projection neurons with terminals in limited numbers of cortical fields [26,27]. What factors might account for BFCC subpopulation specific cholinergic terminal losses is unclear. In the case of calcarine cortex, it is plausible that this may be a “dying back” phenomenon. Cholinergic efferents from the nBM traverse 2 major pathways, one projecting initially anterior and coursing around the corpus callosum and one traveling through the external capsule [2,26]. Some BFCC afferents to calcarine cortex might travel through the anterior projection with their extended length making them particularly vulnerable to metabolic impairments.

Similarly, our results in regions innervated by other cholinergic systems – metathalamus/thalamus (PPN/LTDC), cerebellum (MVN), and striatum (SChIs) – suggest preferential involvement of subpopulations of cholinergic neurons.

We recently reported that cholinergic terminals in components of the cingulo-opercular task control (COTC) network in patients with PD correlated with the degree of cognitive impairment [28]. The identification of age-related cholinergic terminal deficits within the anterior cingulum, thalamus, metathalamus, insula, and caudate nucleus point to greater vulnerability of COTC hubs [29]. The COTC network plays important roles in the maintenance of tonic alertness and task performance [30]. Maintenance of alertness is a critical function subserving multiple higher cognitive domain functions, such as executive functions and memory. Age-associated cholinergic terminal deficits within COTC nodes may provide a partial explanation of why normal aging is associated with declines in cognitive abilities such as processing speed and certain memory, language, visuospatial, and executive functions [31]. Our finding that cholinergic terminals within COTC nodes may be vulnerable to aging effects expands the growing literature that normal aging is associated with loss of large-scale neural network functions [32] and may increase vulnerability to age-associated neurodegenerations, such as Alzheimer’s disease (AD). FEOBV PET has also potential to be used as a diagnostic test for AD or other types of dementia. For example, a recent VAChT [^{18}F]FEOBV PET study found that cholinergic denervation in AD was more accurate and sensitive in differentiating AD from normal controls compared to [^{11}C]-PIB amyloid PET and [^{18}F]-Fluorodeoxyglucose (FDG) tracers [33]. Similarly, our voxel-based metabolic covariance group analysis between AD and DLB using VAChT [^{18}F]FEOBV PET reveals a specific covarying pattern of cholinergic losses in DLB supporting the use of VAChT [^{18}F]FEOBV PET to distinguish DLB from AD [34].

Our results also implicate age-related brain cholinergic deficits in other common age-related clinical phenomena. Given the involvement of the metathalamus and caudate nucleus cholinergic deficits in postural imbalance and falls in PD, cholinergic deficits of these regions in normal aging may increase risk of falling in normal older adults, particularly those taking anti-cholinergic drugs [35]. Our findings emphasize the importance of avoiding anti-cholinergic drugs in the elderly.

Our current findings underscore the notion that brain cholinergic deficits found neurodegenerative disorders such as PD reflect both disease-specific and normal aging-

related degenerative processes. Similar mixed effects of disease and normal aging were shown for nigrostriatal dopaminergic losses in PD [36,37].

There are several limitations of this study. First, gender distribution was not equally distributed across the older (relatively more males) vs. the younger (relatively more females) age groups in the study participants. Our analysis, however, was adjusted for the effects of gender. Furthermore, despite the smaller number of women in the older age group, *post hoc* analysis showed similar regional topographic effects of aging in women in uncorrected analyses. Second, we did not assess the presence of asymptomatic or prodromal biomarkers of Alzheimer and Lewy body disorders, which might have resulted in possible inclusion of otherwise neurologically intact adults in our study.

We conclude that all major cholinergic cell groups and projections, including the BFCC, PPN-LDTC, MVN and SChIs, are vulnerable to effects of normal aging. Our results suggest that subpopulations of these cholinergic systems are particularly vulnerable. Our findings may have clinical implications and may help to explain the deleterious effects of anti-cholinergic drugs in the otherwise neurologically intact elderly without the history of neurological disease.

Acknowledgements

The authors thank Christine Minderovic, Cyrus Sarosh, the PET technologists, cyclotron operators, and radiochemists, for their assistance. We are indebted to the subjects who participated in this study.

Funding

This work was supported by the National Institutes of Health [P01 NS015655, RO1 NS070856, P50 NS091856, P50 NS123067], Department of Veterans Affairs grant [I01 RX001631], the Michael J. Fox Foundation, the Parkinson's Foundation, W. Garfield Weston Foundations' Weston Brain Institute. None of the funding agencies had a role in the design and conduct of the study, in the collection, management, analysis and interpretation of the data, in the preparation, review or approval of the manuscript, nor in the decision to submit the manuscript for publication.

Abbreviations:

AChE	Acetylcholinesterase
BFCC	Basal Forebrain Cholinergic Corticopetal complex
COTC	Cingulo-Opercular Task Control
FEOBV	Fluoroethoxybenzovesamicol
IBVM	Iodobenzovesamicol
MVC	Medial Vestibular Complex
PPN/LDTC	pedunculopontine nucleus/lateral dorsal tegmental complex
PET	Positron Emission Tomography
SChIs	Striatal Cholinergic Interneurons

SPECT	Single Photon Emission Computed Tomography
VAChT	vesicular acetylcholine transporter

References

[1]. Gasiorowska A, Wydrych M, Drapich P, et al. The Biology and Pathobiology of Glutamatergic, Cholinergic, and Dopaminergic Signaling in the Aging Brain. Front Aging Neurosci 2021; 13: 654932021/07/310.3389/fnagi.2021.654931.

[2]. Schmitz TW, Zaborszky L. Chapter 10 - Spatial topography of the basal forebrain cholinergic projections: Organization and vulnerability to degeneration. In: Swaab DF, Kreier F, Lucassen PJ, editors. Handbook of Clinical Neurology. Elsevier; 2021. p. 159–73.

[3]. Candy JM, Perry EK, Perry RH, et al. The current status of the cortical cholinergic system in Alzheimer's disease and Parkinson's disease. Prog Brain Res 1986; 70: 105–132. 1986/01/01. 10.1016/s0079-6123(08)64300-9. [PubMed: 3554348]

[4]. Mesulam MM, Geula C. Nucleus basalis (Ch4) and cortical cholinergic innervation in the human brain: observations based on the distribution of acetylcholinesterase and choline acetyltransferase. J Comparative Neurol 1988; 275: 216–240. 1988/09/08. 10.1002/cne.902750205.

[5]. Heckers S, Geula C, Mesulam M. Cholinergic innervation of the human thalamus: dual origin and differential nuclear distribution. J Comp Neurol 1992;325:68–82. [PubMed: 1282919]

[6]. Zhang C, Zhou P, Yuan T. The cholinergic system in the cerebellum: from structure to function. Rev Neurosci 2016; 27: 769-772016/08/210.1515/revneuro-2016-0008.

[7]. Dautan D, Hacioglu Bay H, Bolam JP, et al. Extrinsic sources of cholinergic innervation of the striatal complex: a whole-brain mapping analysis. Front Neuroanat 2016; 10: 1. 2016/02/03. 10.3389/fnana.2016.00001. [PubMed: 26834571]

[8]. Janickova H, Rosborough K, Al-Onaizi M, et al. Deletion of the vesicular acetylcholine transporter from pedunculopontine/laterodorsal tegmental neurons modifies gait. J Neurochem 2017; 140: 787-792016/11/210.1111/jnc.13910.

[9]. Albin RL, Bohnen NI, Muller M, et al. Regional vesicular acetylcholine transporter distribution in human brain: A [(18) F] fluoroethoxybenzovesamicol positron emission tomography study. J Comp Neurol 2018. doi: 10.1002/cne.24541.

[10]. Petrou M, Frey KA, Kilbourn MR, et al. In vivo imaging of human cholinergic nerve terminals with (-)-5-^{18}F-fluoroethoxybenzovesamicol: biodistribution, dosimetry, and tracer kinetic analyses. J Nucl Med 2014;55:396–404. doi: 10.2967/jnumed.113.124792. [PubMed: 24481024]

[11]. Boertien JM, van der Zee S, Chrysou A, et al. Study protocol of the DUtch PARkinson Cohort (DUPARC): a prospective, observational study of de novo Parkinson's disease patients for the identification and validation of biomarkers for Parkinson's disease subtypes, progression and pathophysiology. BMC Neurol 2020; 20: 245. 2020/06/15. 10.1186/s12883-020-01811-3. [PubMed: 32534583]

[12]. Bohnen NI, Muller ML, Kotagal V, et al. Heterogeneity of cholinergic denervation in Parkinson's disease without dementia. J Cereb Blood Flow Metab 2012; 32: 1609–17. 2012/05/10. 10.1038/jcbfm.2012.60. [PubMed: 22569194]

[13]. Bohnen NI, Kanel P, Koeppe RA, et al. Regional cerebral cholinergic nerve terminal integrity and cardinal motor features in Parkinson's disease. Brain Commun 2021; 3: fcab109. 10.1093/braincomms/fcab109. [PubMed: 34704022]

[14]. Shao X, Hoareau R, Hockley BG, et al. Highlighting the Versatility of the Tracerlab Synthesis Modules. Part 1: Fully Automated Production of [F]Labelled Radiopharmaceuticals using a Tracerlab FX(FN). J Label Compounds Radiopharmaceuticals 2011; 54: 292–307. 2011/07/20. 10.1002/jlcr.1865.

[15]. Thiele F, Young S, Buchert R, et al. Voxel-based classification of FDG PET in dementia using inter-scanner normalization. NeuroImage 2013; 77: 62–9. 2013/04/02. 10.1016/j.neuroimage.2013.03.031. [PubMed: 23541799]

[16]. Kanel P, Müller M, van der Zee S, et al. Topography of cholinergic changes in dementia with Lewy bodies and key neural network hubs. J Neuropsychiatry Clin Neurosci 2020; 32: 370–5. 2020/06/06. 10.1176/appi.neuropsych.19070165. [PubMed: 32498602]

[17]. Nejad-Davarani S, Koeppe RA, Albin RL, et al. Quantification of brain cholinergic denervation in dementia with Lewy bodies using PET imaging with [(18)F]-FEOBV. Mol Psychiatry 2019; 24: 322–327. 2018/08/08. 10.1038/s41380-018-0130-5. [PubMed: 30082840]

[18]. Albin RL, Minderovic C, Koeppe RA. Normal striatal vesicular acetylcholine transporter expression in Tourette syndrome. eNeuro 2017; 4 2017/08/10. 10.1523/ENEURO.0178-17.2017.

[19]. Muller-Gartner HW, Links JM, Prince JL, et al. Measurement of radiotracer concentration in brain gray matter using positron emission tomography: MRI-based correction for partial volume effects. J Cereb Blood Flow Metab 1992; 12: 571–583. 1992/07/01. 10.1038/jcbfm.1992.81. [PubMed: 1618936]

[20]. Amunts K, Mohlberg H, Bludau S, et al. Julich-Brain: a 3D probabilistic atlas of the human brain's cytoarchitecture. Science 2020;369(988–992):20200730. doi: 10.1126/science.abb4588.

[21]. Zilles K, Amunts K. Centenary of Brodmann's map–conception and fate. Nat Rev Neurosci 2010;11(139–145):20100104. doi: 10.1038/nrn2776.

[22]. Zilles K, Schleicher A, Palomero-Gallagher N, et al. 21 - Quantitative Analysis of Cyto- and Receptor Architecture of the Human Brain. In: Toga AW, Mazziotta JC, editors. Brain Mapping: The Methods. San Diego: Academic Press; 2002. p. 573–602.

[23]. Kuhl DE, Koeppe RA, Minoshima S, et al. In vivo mapping of cerebral acetylcholinesterase activity in aging and Alzheimer's disease. Neurology 1999; 52: 691–9. 1999/03/17. DOI: 10.1212/wnl.52.4.691. [PubMed: 10078712]

[24]. Mitsis EM, Cosgrove KP, Staley JK, et al. Age-related decline in nicotinic receptor availability with [(123)I]5-IA-85380 SPECT. Neurobiol Aging 2009; 30: 1490–7. 2008/02/05. 10.1016/j.neurobiolaging.2007.12.008. [PubMed: 18242781]

[25]. Parent M, Bedard MA, Aliaga A, et al. PET imaging of cholinergic deficits in rats using [18F]fluoroethoxybenzovesamicol ([18F] FEOBV). NeuroImage 2012;62(555–561):20120425. doi: 10.1016/j.neuroimage.2012.04.032.

[26]. Zaborszky L, Csordas A, Mosca K, et al. Neurons in the basal forebrain project to the cortex in a complex topographic organization that reflects corticocortical connectivity patterns: an experimental study based on retrograde tracing and 3D reconstruction. Cereb Cortex (New York, NY: 1991) 2015; 25: 118–137. 2013/08/22. 10.1093/cercor/bht210.

[27]. Gielow MR and Zaborszky L. The input-output relationship of the cholinergic basal forebrain. Cell Rep 2017; 18: 1817–30. 2017/02/16. 10.1016/j.celrep.2017.01.060. [PubMed: 28199851]

[28]. van der Zee S, Müller TMML, Kanel P, et al. Cholinergic denervation patterns across cognitive domains in Parkinson's disease. Movement Disord 2021; 36: 642–50. 2020/11/03. DOI: 10.1002/mds.28360. [PubMed: 33137238]

[29]. Power JD, Cohen AL, Nelson SM, et al. Functional network organization of the human brain. Neuron 2011; 72: 665–78. 2011/11/22. 10.1016/j.neuron.2011.09.006. [PubMed: 22099467]

[30]. Sadaghiani S and D'Esposito M. Functional characterization of the Cingulo-opercular network in the maintenance of tonic alertness. Cereb cortex (New York, NY: 1991) 2015; 25: 2763–73. 2014/04/29. 10.1093/cercor/bhu072.

[31]. Harada CN, Natelson Love MC and Triebel KL. Normal cognitive aging. Clin Geriatr Med 2013; 29: 737–52. 2013/10/08. 10.1016/j.cger.2013.07.002. [PubMed: 24094294]

[32]. Zhang HY, Chen WX, Jiao Y, et al. Selective vulnerability related to aging in large-scale resting brain networks. PLoS One 2014; 9: e108807. 2014/10/02. 10.1371/journal.pone.0108807. [PubMed: 25271846]

[33]. Aghourian M, Legault-Denis C, Soucy JP, et al. Quantification of brain cholinergic denervation in Alzheimer's disease using PET imaging with [(18)F]-FEOBV. Mol Psychiatry 2017; 22: 1531–1538. 2017/09/13. 10.1038/mp.2017.183. [PubMed: 28894304]

[34]. Kanel P, Bedard M-A, Aghourian M, et al. Molecular imaging of the cholinergic system in alzheimer and lewy body dementias: expanding views. Curr Neurol Neurosci Rep 2021;21:52. doi: 10.1007/s11910-021-01140-z. [PubMed: 34545424]

[35]. Bohnen NI, Kanel P, Koeppe RA, et al. Regional cerebral cholinergic nerve terminal integrity and cardinal motor features in Parkinson's disease. Brain Commun 2021; 3. ARTN fcab1091093/braincomms/fcab10910.1093/braincomms/fcab109.

[36]. de la Fuente-Fernandez R, Schulzer M, Kuramoto L, et al. Age-specific progression of nigrostriatal dysfunction in Parkinson's disease. Ann Neurol 2011; 69: 803–10. 2011/01/20. 10.1002/ana.22284. [PubMed: 21246604]

[37]. Rodriguez M, Rodriguez-Sabate C, Morales I, et al. Parkinson's disease as a result of aging. Aging Cell 2015; 14: 293–308. 2015/02/14. 10.1111/acel.12312. [PubMed: 25677794]

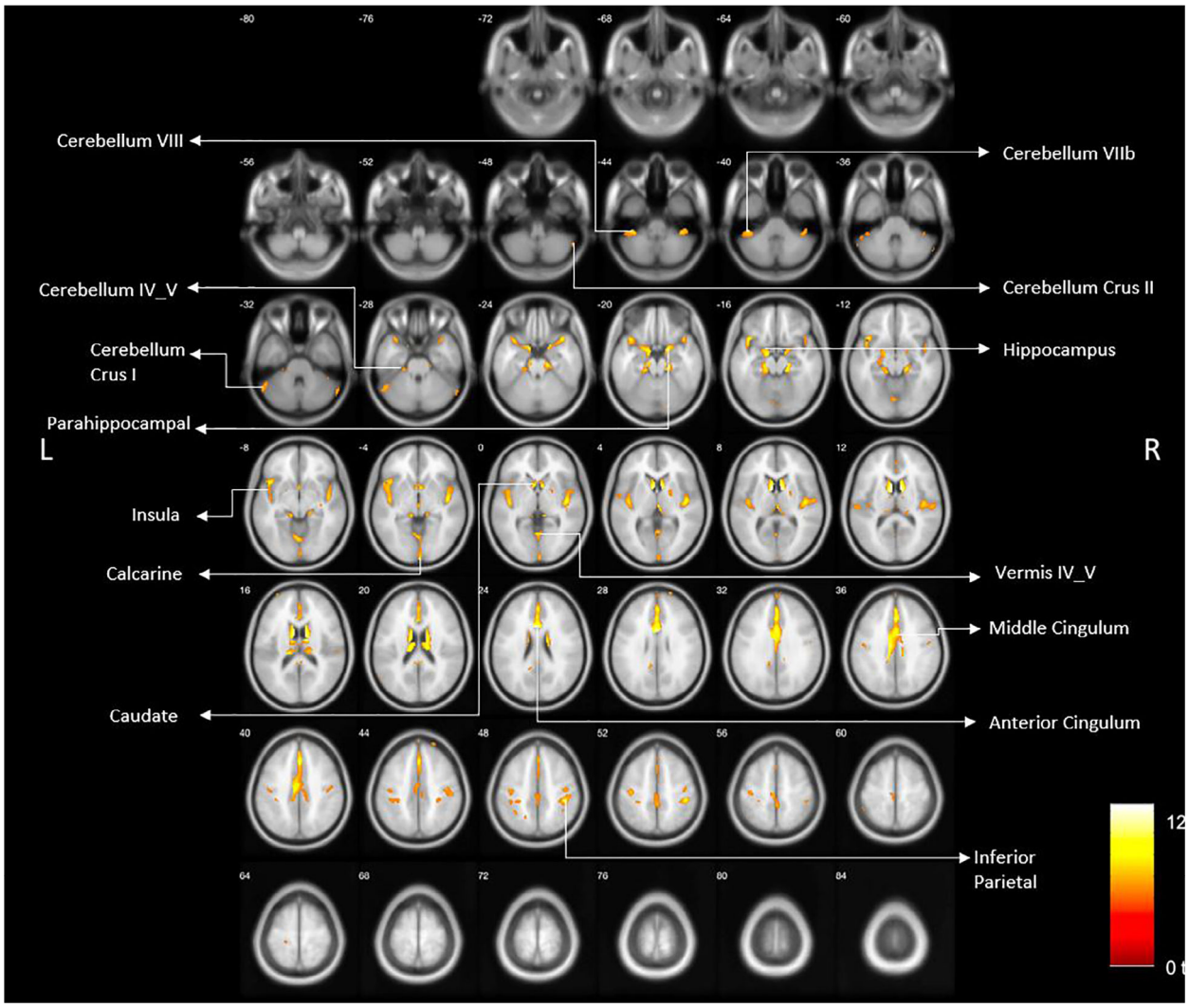

Fig. 1.

Age-related reduced VAChT binding reductions are shown in primary sensorimotor cortex, visual cortex, caudate nucleus, anterior to mid cingulum, bilateral insula, *para*-hippocampus, hippocampus, anterior temporal lobes/amygdala, epithalamus, and cerebellum (gender and FWE-corrected, $P < 0.05$).

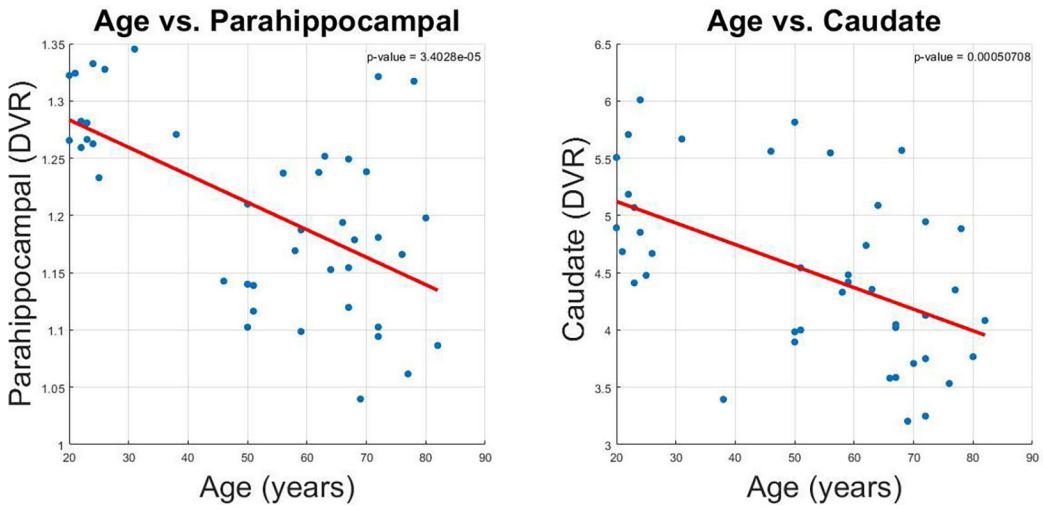

Fig. 2.

Scatter plot of the DVR of parahippocampal gyrus and caudate nucleus with age.

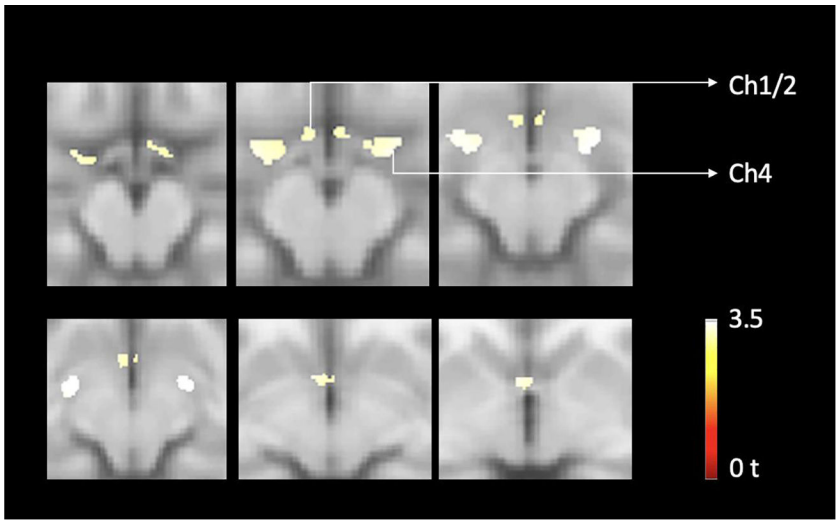

Fig. 3.

Voxel-based analysis of basal forebrain loss over time in neurologically intact elderly. Findings show evidence of significant age-associated cholinergic forebrain volume losses in neurologically intact adults, FWE-corrected $P < 0.05$.

Table 1

Table 1 lists of significant age-associated FEOBV PET clusters with a minimum of 50 voxels with the location of the peak voxel, peak voxel z and t-score, and the regions associated with the clusters.

Clusters (voxels)	P	Peak MNI coordinates [x,y,z]	Z	T	Regions
1146	<0.001	−6 8 10	7.8	12.28	Left and Right Caudate
					Left and Right Thalamus
					Left and right lateral geniculate nuclei
					Left and right medial geniculate nuclei
					Left and Right Olfactory
2289	<0.001	−2 8 26	7.58	11.57	Left and Right Mid Cingulum
					Left and Right Ant Cingulum
					Left and Right Precuneus
					Left and Right Supp Motor Area
					Left and Right Frontal sup medial
					Left and Right paracentral lobule
					Left post cingulum
244	<0.001	18 −24 −18	6.74	9.37	Right Parahippocampal
					Right Lingual
					Right Cerebellum lobules 3, 4 & 5
					Right Hippocampus
					Right Fusiform gyrus
967	<0.001	44 −12 2	6.72	9.33	Right Insula
					Right Temporal sup
					Right Heschl gyrus
					Right temporal superior pole
					Right parahippocampal gyrus
					Right Rolandic operculum
					Right Amygdala
					Right Hippocampus
					Right frontal inferior orbitofrontal lobe
1386	<0.001	−14 −8 −16	6.52	8.86	Left Hippocampus

Clusters (voxels)	P	Peak MNI coordinates [x,y,z]	Z	T	Regions
					Left Superior temporal pole
					Left Insula
					Left Parahippocampal gyrus
					Left Frontal inferior orbitofrontal lobe
					Left Heschl gyrus
					Left Amygdala
					Left Cerebellum lobules 3, 4 &5
					Left Olfactory cortex
					Left Rolandic operculum
					Left fusiform gyrus
					Left lingual gyrus
					Left inferior frontal gyrus triangular part
362	<0.001	42 −34 50	6.49	8.79	Right postcentral cortex
					Right precentral cortex
					Right inferior parietal lobe
36	<0.001	2 −38 18	6.13	8.02	Left and Right posterior cingulate cortex
267	<0.001	0 −60 2	6.12	7.99	Vermis sections of lobules 4, 5 & 6
					Left and right lingual gyrus
					Left Cerebellum lobules 4, 5 & 6
					Left and Right Calcarine cortex
308	<0.001	−40 −38 −42	5.72	7.33	Left Cerebellum Crus 1 & 2
					Left Cerebelum lobules 7b & 8
					Left Inferior Temporal lobe
102	<0.001	40 −40 −42	5.84	7.44	Right Cerebellum Crus 1 & 2
					Right Cerebellum lobules 7b & 8
157	<0.001	−40 −20 52	5.69	7.16	Left Postcentral cortex
					Left Precentral cortex
110	<0.001	4 −98 −4	5.68	7.15	Left Calcarine cortex
129	0.007	−30 −34 50	5.08	6.10	Left Postcentral cortex
					Left Inferior parietal cortex
50	0.002	58 −66 −32	5.35	6.55	Right Cerebellum Crus1

Clusters (voxels)	P	Peak MNI coordinates [x,y,z]	Z	T	Regions
51	0.004	−56 −22 12	5.24	6.36	Left superior temporal lobe
					Left postcentral cortex
					Left supramarginal gyrus
53	0.004	20 2 4	5.21	6.32	Right Putamen
					Right Pallidum